Journal of Organometallic Chemistry 693 (2008) 3741–3750

Contents lists available at ScienceDirect

Journal of Organometallic Chemistry

journal homepage: www.elsevier.com/locate/jorganchem

Syntheses of *rac/meso*-{PhP(3-*t*-Bu-C_5H_3)$_2$}-Zr{RN(CH_2)$_3$NR}, structural analyses of *rac*-{PhP(3-*t*-Bu-C_5H_3)$_2$}Zr{RN(CH_2)$_3$NR} (where R is $SiMe_3$ or Ph), and *meso* to *rac* isomerization

Jonathan C. Axtell, Susan D. Thai, Laurel A. Morton, William S. Kassel, William G. Dougherty, Deanna L. Zubris *

Department of Chemistry, Mendel Science Center, Villanova University, Villanova, PA 19085, United States

ARTICLE INFO

Article history:
Received 8 August 2008
Received in revised form 5 September 2008
Accepted 5 September 2008
Available online 18 September 2008

Keywords:
Zirconocene
Cyclopentadienyl
Phosphine
Synthesis
X-ray structure

ABSTRACT

Syntheses of *rac/meso*-{PhP(3-*t*-Bu-C_5H_3)$_2$}Zr{$Me_3SiN(CH_2)_3NSiMe_3$} (***rac*-3**/***meso*-3**) and *rac/meso*-{PhP(3-*t*-Bu-C_5H_3)$_2$}Zr{PhN(CH_2)$_3$NPh} (***rac*-4**/***meso*-4**) were achieved by metallation of K_2[PhP(3-*t*-Bu-C_5H_3)$_2$] · 1.3 THF (**2**) with Zr{RN(CH_2)$_3$NR}Cl_2(THF)$_2$ (where R = $SiMe_3$ or Ph, respectively) using ethereal solvent. These isomeric pairs were characterized by ^{1}H, ^{13}C{^{1}H}, and ^{31}P{^{1}H} NMR spectroscopy; ***rac*-3** and ***rac*-4** were also examined via single crystal X-ray crystallography. The structures of ***rac*-3** and ***rac*-4** are notable in the tendency of the cyclopentadienyl rings towards η^3 coordination. While isolated samples of ***rac*-3**/***meso*-3** and ***rac*-4**/***meso*-4** slowly isomerize in tetrahydrofuran-d_8 to equilibrium ratios, the isomerization rate for **3** is more than 15-fold greater than that for **4**. In addition, equilibrium ratios are rapidly reached when isolated samples of ***rac*-3**/***meso*-3** and ***rac*-4**/***meso*-4** are exposed to tetrabutylammonium chloride in tetrahydrofuran-d_8 solvent. We propose that a nucleophile (either chloride or the phosphine interannular linker) brings about dissociation of one cyclopentadienyl ring, thus promoting the *rac/meso* isomerization mechanism.

1. Introduction

A wide range of group 4 metallocenes and metallocene analogs have been synthesized and tested as precatalysts for polymerization of ethylene, propylene, and other α-olefins [1]. From this wealth of polymerization data, defined relationships between precatalyst symmetry and polymer tacticity have emerged [2]. Symmetry may be enforced by use of an interannular bridge, or linker, between the two cyclopentadienyl rings of these metallocenes. *Ansa*-metallocenes [3] differ electronically from their unlinked counterparts; these differences were recently scrutinized in the literature [4]. Choice of interannular linker and its effect on reactivity was the subject of a recent review [5].

Over the past eight years, Jordan and coworkers [6] have described the chelate-controlled synthesis of a wide range of *ansa*-zirconocenes (with substituted bis(cyclopentadienyl) or bis(indenyl) ligands incorporating a Me_2Si, or in one case, a CH_2CH_2, interannular bridge). The importance of metallation agent and solvent selection was highlighted in Ref. [6c], where the chelate-controlled synthesis of *meso*- and *rac*-Me_2Si(3-*t*-Bu-C_5H_3)$_2$Zr{RN(CH_2)$_3$NR} (where R is Ph or $SiMe_3$, respectively) was presented (Fig. 1). The chelating bis(amide) ligand accounts for the differing diastereomeric outcomes of these metallations. While the {Me_3SiN-(CH_2)$_3$N$SiMe_3$} ligand adopts a twist conformation, best suited to the *rac*-isomer, the {PhN(CH_2)$_3$NPh} ligand can, in some cases, adopt an envelope confirmation to accommodate the steric requirements of the *meso* isomer; these diastereomeric preferences were the subject of a recent DFT study [6e]. Solvent choice is critical for isolation of a single diastereomer in these chelate-controlled metallations. For example, use of the mismatched metallation agent/solvent pair, Zr{PhN(CH_2)$_3$NPh}Cl_2(THF)$_2$/tetrahydrofuran, provides a *rac/meso* mixture of products [6f]. Jordan et al. propose that the solvent effect stems from differing solubility of the lithium chloride reaction byproduct; chloride ion catalyzes isomerization of the *meso* isomer to the more thermodynamically stable *rac* isomer.

We sought to employ Jordan's methodology for the preparation of *rac*- and *meso*-*ansa*-zirconocenes with a phenyl-phosphine interannular bridge. Ligands (such as ([Me_2P(fluorenyl)$_2$]$^-$) [7] and [R_2P(2-Me-4-*t*-Bu-C_5H_2)$_2$]$^-$ where R = Me or *n*-Bu [8]) and group 4 metallocenes with a phosphorus-containing *ansa*-bridge are the subject of two recent review articles [9,10]. A few of these group 4 *ansa*-metallocenes have been tested as ethylene [11–13] and α-olefin polymerization precatalysts [14] (Fig. 2). Other group 4 metallocene dichlorides with a phosphorus-containing *ansa*-bridge have been reported with no mention of their use as

* Corresponding author. Tel.: +1 610 519 4874; fax: +1 610 519 7167.
E-mail address: deanna.zubris@villanova.edu (D.L. Zubris).

0022-328X/$ - see front matter © 2008 Elsevier B.V. All rights reserved.
doi:10.1016/j.jorganchem.2008.09.018

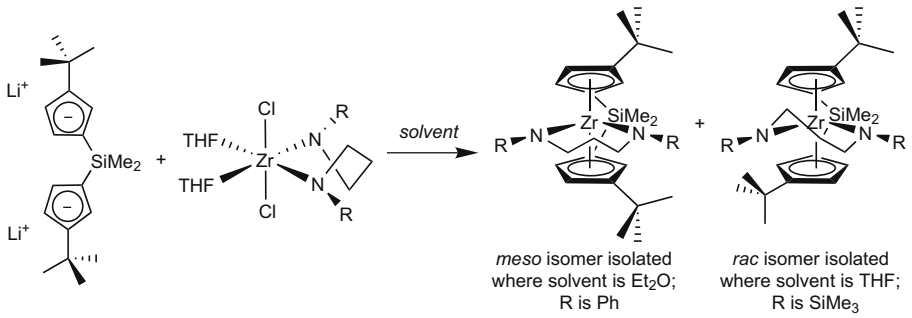

Fig. 1. Choice of metallation agent, $Zr\{RN(CH_2)_3NR\}Cl_2(THF)_2$ (where R is Ph or $SiMe_3$), and reaction solvent (Et_2O or THF) allows for isolation of either *meso*- or *rac*-$Me_2Si(3\text{-}t\text{-}Bu\text{-}C_5H_3)_2Zr\{RN(CH_2)_3NR\}$ (where R is Ph or $SiMe_3$, respectively) [6c].

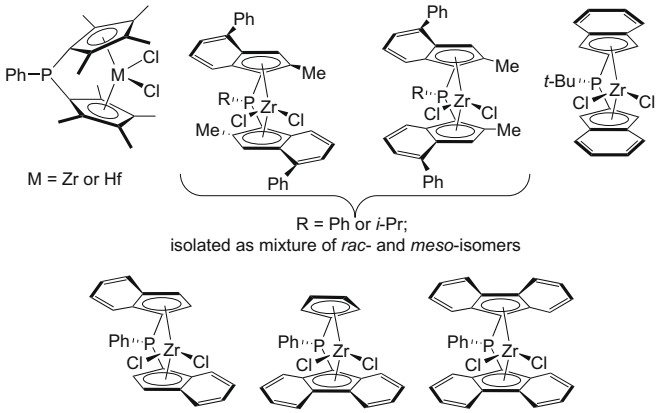

Fig. 2. Group 4 *ansa*-metallocene ethylene and/or propylene polymerization precatalysts incorporating a phosphine-containing interannular bridge: $[PhP(C_5Me_4)_2]MCl_2$ (where M = Zr or Hf) [12], *rac/meso*-$[PhP(2\text{-}Me\text{-}4\text{-}Ph\text{-}indenyl)_2]ZrCl_2$, *rac/meso*-$[(i\text{-}PrP)(2\text{-}Me\text{-}4\text{-}Ph\text{-}indenyl)_2]ZrCl_2$ [14], $[t\text{-}BuP(2\text{-}indenyl)_2]ZrCl_2$ [13], *rac*-$PhP(indenyl)_2ZrCl_2$, $PhP[(fluorenyl)(Cp)]ZrCl_2$ [14], and $PhP(fluorenyl)_2ZrCl_2$ [11,14].

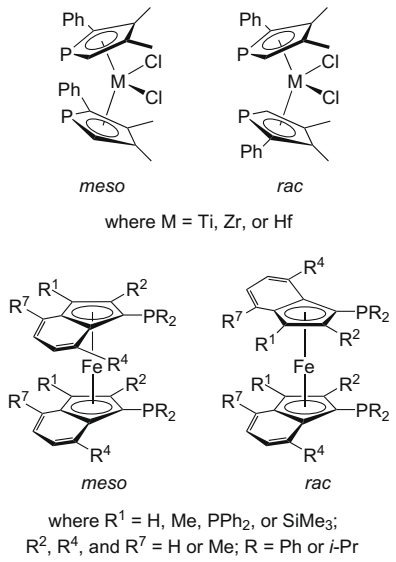

Fig. 3. *Meso/rac* isomer pairs of bis(phosphoyl)zirconocenes described by Hollis [22] and Fu [23], titanocenes described by Hollis [22], hafnocenes described by Fu [23], and bis(phosphino-η^5-indenyl)iron(II) complexes described by Curnow [24].

polyolefin precatalysts, including $[PhP(fluorenyl)_2]HfCl_2$ [11], $[Ph(E)P(C_5Me_4)_2]MX_2$ (where M = Zr or Hf; E = O, S, or Se) [12], $[PhP(2\text{-}indenyl)_2]ZrCl_2$ [13], $[PhP(C_5H_4)_2]TiCl_2$ [15], $[RP(C_5H_4)_2]ZrCl_2$ (where R = Me, Et, *i*-Pr, or *t*-Bu) [16], $[PhP(C_5H_4)_2]ZrCl_2$ [17], $\{[Me_2P(C_5Me_4)_2]MCl_2\}^+$ (where M = Zr or Hf) [18], and *rac/meso*-$\{[R_2P(2\text{-}Me\text{-}4\text{-}t\text{-}Bu\text{-}C_5H_2)_2]ZrCl_2\}^+$ (where R = Me or *n*-Bu) [19]. Also, phosphorus has been used as a component of multi-atom interannular bridges for *ansa*-zirconocenes, such as $[\{Me_2P(C_5H_4)\}\{Cl_2B(C_5H_4)\})]ZrCl_2$, $[\{Et_2P(2\text{-}Me\text{-}indenyl)\}\{Cl_2B(2\text{-}methylindenyl)\})]ZrCl_2$ [20], and $[PhP(CH_2CH_2\text{-}\eta^5\text{-}C_5H_4)_2]ZrCl_2$ [21].

We were drawn to the phosphine interannular linker due to its pyramidal nature and ability to enforce two different steric environments at the rear of the metallocene wedge. This feeds into one long-term goal of our research program; namely, the design and testing of complexes to probe the steric requirements for regiocontrol in α-olefin polymerization. It follows that the ability to isolate a single diastereomeric zirconocene (*rac* or *meso*) is critical for meaningful polymerization trials in this vein.

The inclusion of phosphorus in our ligand array introduces the potential for phosphorus-mediated *meso*- to *rac*-isomerization in addition to the possibility of chloride catalyzed *rac/meso* isomerization as described by Jordan (vide supra) [6f]. Hollis [22] and Fu [23] have implicated the role of phosphorus in a ring slip-inversion-ring slip mechanism of isomerization for bis(phosphoyl)titanium, zirconium and hafnium(IV) complexes (Fig. 3). Curnow [24] proposes the following stepwise mechanism for *rac*/*meso* isomerization of bis(phosphino-η^5-indenyl)iron(II) complexes (Fig. 3): tetrahydrofuran-assisted indenyl ring slip, phosphorus coordination, indenide dissociation, indenide recoordination, phosphorus decoordination, and ring slip. Herein, we will describe the synthesis and characterization of *rac/meso*-$PhP(3\text{-}t\text{-}Bu\text{-}C_5H_3)_2Zr\{RN(CH_2)_3NR\}$ (where R = $SiMe_3$ or Ph) and will present our observations of *meso* to *rac* isomerization in these systems. Pure *rac*-$PhP(3\text{-}t\text{-}Bu\text{-}C_5H_3)_2Zr\{RN(CH_2)_3NR\}$ (where R = $SiMe_3$ or Ph) can be isolated (either via controlled isomerization or preferential crystallization); these complexes will be employed in future work directed towards α-olefin polymerization.

2. Results and discussion

Synthesis of our target ligand, $K_2[PhP(3\text{-}t\text{-}Bu\text{-}C_5H_3)_2] \cdot 1.3$ THF (**2**), was achieved via standard methods as described in Scheme 1. Treatment of a solution of $Li(t\text{-}Bu\text{-}C_5H_4)$ (tetrahydrofuran/pentane, 3:1, v/v) with a tetrahydrofuran solution of dichlorophenylphosphine provided neutral compound, $PhP(3\text{-}t\text{-}Bu\text{-}C_5H_4)_2$ (**1**) as a mixture of double bond isomers [25]. Characterization via multinuclear NMR spectroscopy (^1H, ^{13}C, and ^{31}P) verified the presence of these isomers; due to overlapping NMR signals throughout all three spectra, individual isomer identities were not assigned. Compound **1** can be doubly deprotonated by addition of 2 equiv. of either potassium bis(trimethylsilylamide) or potassium *tert*-butox-

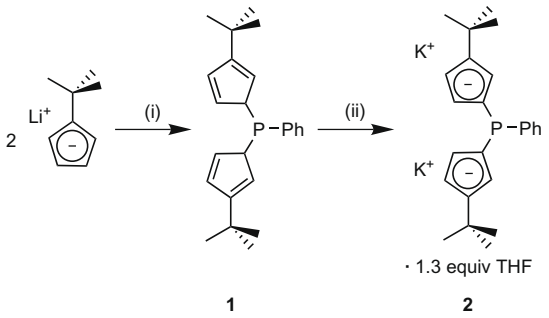

Scheme 1. Reagents and conditions: (i) chlorodiphenylphosphine, THF/pentane, −78 °C → 22 °C, 18 h; (ii) 2 equiv. potassium *tert*-butoxide, THF, 0 °C → 22 °C, 72 h.

ide to yield $K_2[PhP(3\text{-}t\text{-}Bu\text{-}C_5H_3)_2] \cdot 1.3$ THF (**2**) as a white powder. We found preparation and isolation of a dipotassio salt preferable to a dilithio salt due to persistent impurities observed upon isolation of the dilithio salt; the analogous preparation of a disodium salt was not attempted. ^{1}H NMR analysis of **2** reveals the presence of nonstoichiometric protio THF (1.3 equiv.); poor solubility of **2** in THF has precluded preparative scale recrystallizations for elemental analysis purposes.

tion were obtained from such a solution cooled to –35 °C for 8 days (Fig. 4).

As expected, the $\{Me_3SiN(CH_2)_3NSiMe_3\}$ chelate adopts a twist conformation, as observed previously for *rac*-$Me_2Si(3\text{-}t\text{-}Bu\text{-}C_5H_3)_2Zr\{Me_3SiN(CH_2)_3NSiMe_3\}$ [6c]. The following deviations in Å of C and Si atoms from the N(1)–Zr–N(2) plane are consistent with the twist conformation: Si(1) −0.70, C(28) +0.73, C(29) −0.10, C(30) −0.86, Si(2) +0.60. Another similarity with *rac*-$Me_2Si(3\text{-}t\text{-}Bu\text{-}C_5H_3)_2Zr\{Me_3SiN(CH_2)_3NSiMe_3\}$ is the slight displacement of both *t*-butyl substituents out of the cyclopentadienyl ring planes, away from the zirconium. The most notable aspect of ***rac*-3** is the trend towards η^3-coordination of the cyclopentadienyl rings, evidenced by the 2.481–2.836 Å range of Zr–C(cyclopentadienyl) bond lengths (as compared to the 2.495–2.796 Å range of Zr–C bond lengths for dimethylsilyl-bridged *rac*-$Me_2Si(3\text{-}t\text{-}Bu\text{-}C_5H_3)_2Zr\{Me_3SiN(CH_2)_3NSiMe_3\}$ [6c] and the 2.435–2.608 Å range of Zr–C bond lengths for phenylphosphine-bridged $[PhP(C_5Me_4)_2]ZrCl_2$ [12]). In fact, various angles (Fig. 5) make the coordination mode of the cyclopentadienyl rings in ***rac*-3** more consonant with doubly-linked, as opposed to singly-linked, zirconocenes [26]. For example, the following centroid–Zr–centroid angles (γ) are reported for select singly-linked zirconocenes: for *rac*-$Me_2Si(3\text{-}t\text{-}Bu\text{-}C_5H_3)_2Zr\{Me_3SiN(CH_2)_3NSiMe_3\}$ [6c], $\gamma = 122.5(9)°$;

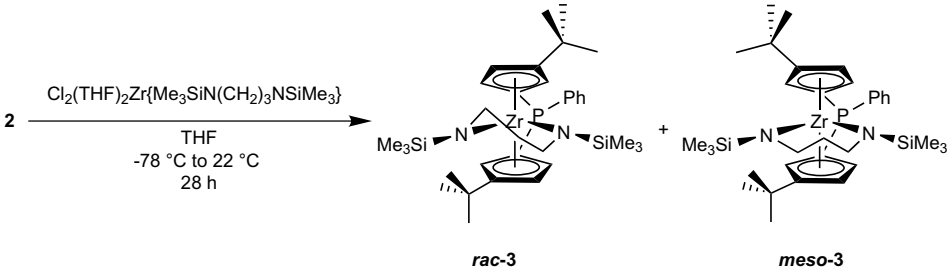

(1)

Preparative scale metallation of $K_2[PhP(3\text{-}t\text{-}Bu\text{-}C_5H_3)_2] \cdot 1.3$ THF (**2**) with $Zr\{Me_3SiN(CH_2)_3NSiMe_3\}Cl_2(THF)_2$ in tetrahydrofuran solvent over the course of 28 h provides both *rac*- and *meso*-$PhP(3\text{-}t\text{-}Bu\text{-}C_5H_3)_2Zr\{Me_3SiN(CH_2)_3NSiMe_3\}$ (***rac*-3/*meso*-3**) as a pale yellow microcrystalline solid in a 2:1 isomeric ratio (Eq. (1)). The pyramidal geometry at phosphorus is evidenced by the number of inequivalent ^{1}H NMR resonances in this *rac*/*meso* mixture. For example, ***rac*-3** displays six cyclopentadienyl signals, two trimethylsilyl methyl signals, and two *tert*-butyl methyl signals. The upfield ^{31}P NMR chemical shifts for ***meso*-3** and ***rac*-3** (−43.6 (*meso*) and −37.1 (*rac*) in benzene-d_6 solvent; −40.3 (*meso*) and −33.8 (*rac*) in THF-d_8 solvent) are consistent with those reported for related phosphine-bridged zirconocenes [12,14,17]. COSY and HETCOR methods were used to assist with NMR peak assignments. While the pyramidal geometry at phosphorus creates the possibility of two distinct *meso* isomers (one with the phosphorus-phenyl substituent on the same side of the zirconocene as the *t*-butyl substituents, and the other with the phosphorus-phenyl on the opposite side of the zirconocene as the *t*-butyl substituents), only one of these *meso* isomers is detected under our experimental conditions. Based on steric arguments, one would expect the latter to be the preferred *meso* isomer (as depicted in Eq. (1)). The *rac*-isomer preferentially crystallizes from a concentrated pentane solution of ***rac*-3/*meso*-3**; indeed, single crystals of ***rac*-3** suitable for X-ray diffrac-

for $[PhP(C_5Me_4)_2]ZrCl_2$ [12], $\gamma = 125.9°$; and for ***rac*-3**, $\gamma = 120.2°$. Further, the centroid–Zr–centroid angle, interplanar ring angle ($\alpha = 73.6°$), Cp(normal)–Cp(normal) dihedral angle ($\beta = 106.4°$), and tilt angle ($\tau = 6.9°$) for ***rac*-3** are very similar to that of doubly-linked $[(Me_2Si)_2(3,5\text{-}i\text{-}Pr_2Cp)(4\text{-}i\text{-}PrCp)]ZrCl_2$ (where $\gamma = 120.3°$, $\alpha = 73.9°$, $\beta = 106.1°$, and $\tau = 7.1°$). [27] Since the success of doubly-linked $[(Me_2Si)_2(3,5\text{-}i\text{-}Pr_2Cp)(4\text{-}i\text{-}PrCp)]ZrCl_2$ as an α-olefin polymerization precatalyst has been, at least in part, attributed to these characteristic angles, we are encouraged that ***rac*-3** may display similar angles upon conversion to a zirconocene dichloride (presumed) precatalyst for α-olefin polymerization.

We have followed the course of the reaction described in Eq. (1) by ^{1}H and ^{31}P NMR spectroscopy. At 22 °C, the metallation reaction is rapid; upon thawing a frozen sample of **2** and $Zr\{Me_3SiN(CH_2)_3NSiMe_3\}Cl_2(THF)_2$ in tetrahydrofuran-d_8 solvent, **2** is immediately consumed to provide a mixture of ***rac*-3** and ***meso*-3** (in a 3:2 ratio, with slightly more *meso* isomer than our preparative scale metallation). Over the course of days, the proportion of ***rac*-3** increases at the expense of ***meso*-3**. In separate reaction trials, we found that the presence of excess $Zr\{Me_3SiN(CH_2)_3NSiMe_3\}Cl_2(THF)_2$ or substoichiometric **1** (presumably formed via partial hydrolysis of **2** during sample preparation) facilitates isomerization, and over the course of 1 day in each case provides a sample that is 100% ***rac*-3** (within the detection

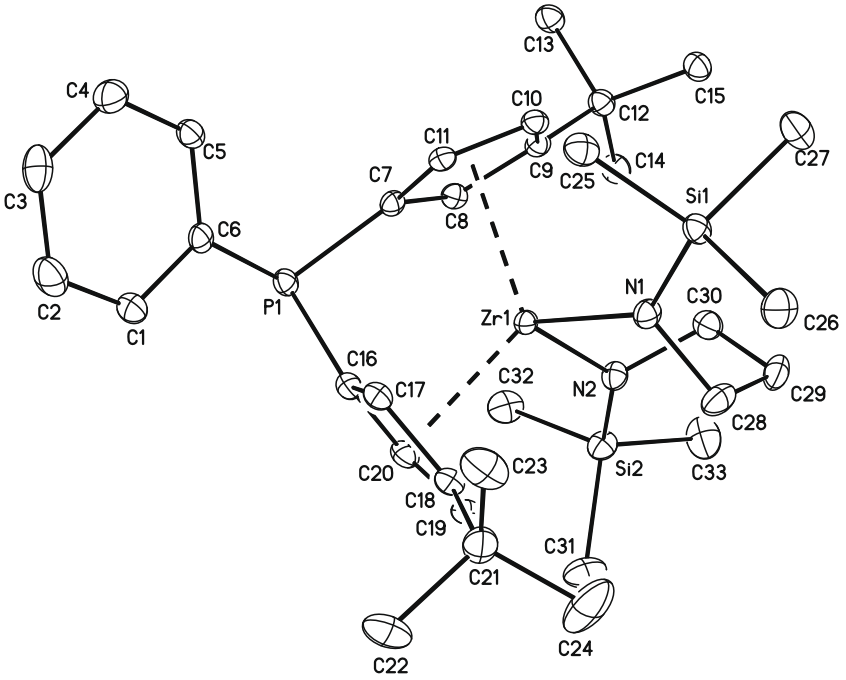

Fig. 4. X-ray crystal structure of ***rac*-3**. Selected bond distances (Å) and angles (deg): Zr(1)–N(1), 2.096(2); Zr(1)–N(2), 2.107(2); N(1)–Si(1), 1.733(2); N(2)–Si(2), 1.735(2); Zr(1)–C(7), 2.503(3); Zr(1)–C(8), 2.665(3); Zr(1)–C(9), 2.836(3); Zr(1)–C(10), 2.683(3); Zr(1)–C(11), 2.481(3); Zr(1)–C(16), 2.519(3); Zr(1)–C(17), 2.586(3); Zr(1)–C(18), 2.754(3); Zr(1)–C(19), 2.655(3); Zr(1)–C(20), 2.523(3); Zr(1)–{C(7)–C(11) centroid}, 2.346; Zr(1)–{C(16)–C(20) centroid}, 2.314; N(1)–Zr(1)–N(2), 93.95(9); centroid–Zr–centroid, 120.2.

limit for NMR integration). The data from a representative reaction trial (with excess $Zr\{Me_3SiN(CH_2)_3NSiMe_3\}Cl_2(THF)_2$ present) is given in Fig. 6. To further probe the role of phosphine in the isomerization mechanism, triphenylphosphine (1 equiv.) was added to one of our metallation trials. However, triphenylphosphine thwarts the desired metallation reaction; ***rac*-3** and ***meso*-3** were not observed.

The metallation described in Eq. (1) was also tracked at low temperature (−30 °C) in tetrahydrofuran-d_8 solvent. Immediately, upon thawing a frozen sample of **2** and $Zr\{Me_3SiN(CH_2)_3NSiMe_3\}Cl_2(THF)_2$ in tetrahydrofuran-d_8 solvent, new signals appear in both the ^1H and ^{31}P NMR spectra corresponding to unidentified intermediate/s (the number and chemical shift range of the ^{31}P signals suggest the intermediate/s have structural similarity to **1**), and after 45 min at −30 °C, broad signals appear for ***rac*-3** and ***meso*-3** (in an approximate 3:2 ratio). Upon warming to 0 °C, these signals continue to slowly increase in intensity; further warming to 25 °C leads to complete consumption of starting materials while maintaining the initially observed *rac/meso* isomer ratio. Over the course of days at 22 °C, the amount of *rac* isomer increases at the expense of *meso* isomer.

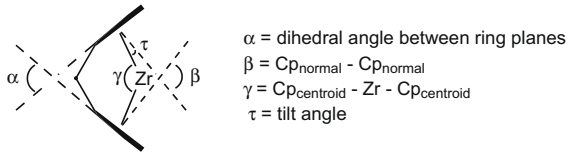

Fig. 5. Definition of α, β, γ, and τ for *ansa*-zirconocenes [4].

We decided to test whether or not the $Zr\{PhN(CH_2)_3NPh\}Cl_2(THF)_2$/diethyl ether combination would allow for the preparative scale isolation of pure ***meso*-4** (Eq. (2)). Metallation of $K_2[PhP(3\text{-}t\text{-}Bu\text{-}C_5H_3)_2]\cdot 1.3$ THF (**2**) with $Zr\{PhN(CH_2)_3NPh\}Cl_2(THF)_2$ in diethyl ether at 0 °C over the course of 2 hours provides both *rac*- and *meso*-$PhP(3\text{-}t\text{-}Bu\text{-}C_5H_3)_2Zr\{PhN(CH_2)_3NPh\}$ (***rac*-4**/***meso*-4**) as an orange-red microcrystalline solid in a 0.36:1.0 isomeric ratio (Eq. (2)). Again, the pyramidal geometry at phosphorus is evidenced by the number of inequivalent ^1H NMR resonances in this *rac/meso* mixture; COSY and HETCOR methods were used to assist with NMR peak assign-

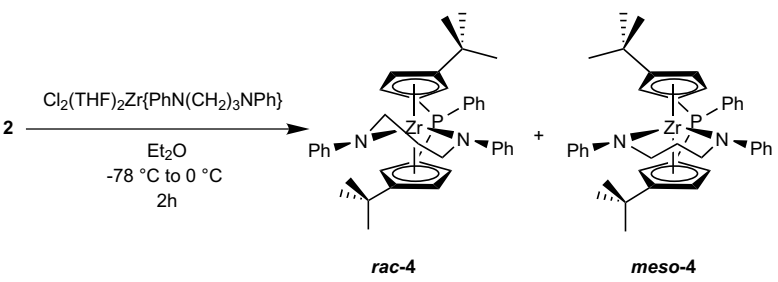

(2)

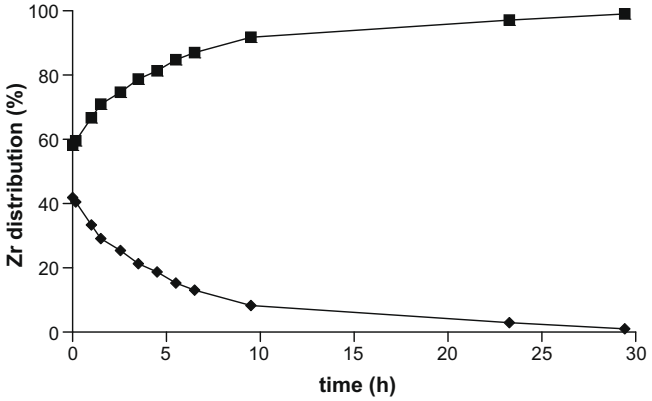

Fig. 6. Formation of ***rac*-3**/***meso*-3** mixture by combination of **2** and excess $Zr\{Me_3SiN(CH_2)_3NSiMe_3\}Cl_2(THF)_2$ (time = 0) and subsequent conversion of the ***meso*-3**/***rac*-3** mixture to ~100% ***rac*-3** (THF-d_8, 22 °C, in the dark). ***rac*-3** (squares, upper curve); ***meso*-3** (diamonds, lower curve).

ments. The deshielded ^{31}P NMR chemical shifts for ***meso*-4** and ***rac*-4** (−38.7 (*meso*) and −35.8 (*rac*) in benzene-d_6 solvent) are similar to those reported for ***meso*-3**/***rac*-3**. Another species was also detected with a ^{31}P NMR chemical shift of −24.6 ppm, a single *t*-butyl methyl ^1H NMR signal, and other ^1H NMR signals that overlap with those of ***meso*-4**/***rac*-4**. The chemical shift difference of this species relative to ***rac*-4**/***meso*-4** is not pronounced enough to suggest oxidation of the phosphine linker (for example, $[Ph(O)P(C_5Me_4)_2]ZrCl_2$ has a ^{31}P NMR signal at +17.9 ppm in benzene-d_6 solvent [12]). It is conceivable that this species is the other potential *meso* isomer of **4**, with the phosphorus-phenyl substituent on the same side of the zirconocene as the *t*-butyl substituents (not pictured in Eq. (2)), though our experiments to date have not allowed us to obtain samples sufficiently enriched in this species to carry out complete NMR characterization.

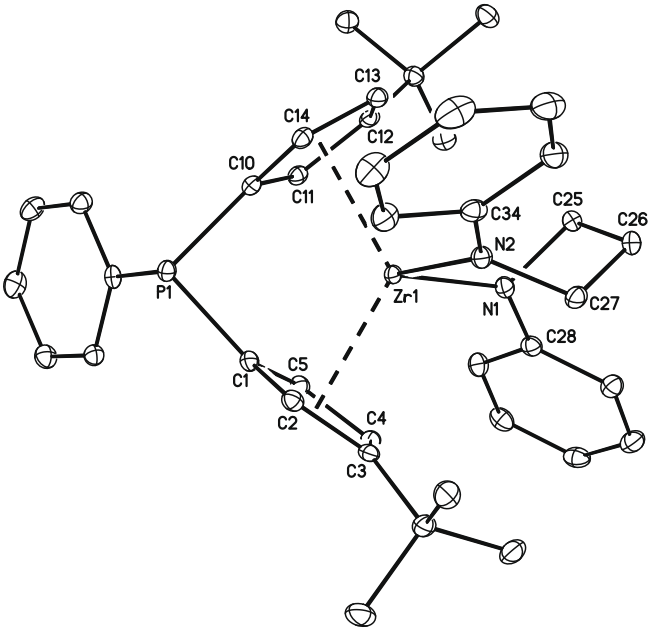

Fig. 7. X-ray crystal structure of ***rac*-4**. Selected bond distances (Å) and angles (deg): Zr(1)–N(1), 2.0956(15); Zr(1)–N(2), 2.1413(15); N(1)–C(28), 1.406(2); N(2)–C(34), 1.404(2); Zr(1)–C(1), 2.4976(17); Zr(1)–C(2), 2.5967(17); Zr(1)–C(3), 2.7211(17); Zr(1)–C(4), 2.6290(18); Zr(1)–C(5), 2.4958(17); Zr(1)–C(10), 2.5063(17); Zr(1)–C(11), 2.5620(17); Zr(1)–C(12), 2.7317(17); Zr(1)–C(13), 2.6337(18); Zr(1)–C(14), 2.5131(17); Zr(1)–{C(1)–C(5) centroid}, 2.291; Zr(1)–{C(10)–C(14) centroid}, 2.293; N(1)–Zr(1)–N(2), 89.45(6); centroid–Zr–centroid, 120.6.

Similar to the ***rac*-3**/***meso*-3** mixture, the *rac* isomer preferentially crystallizes from solutions of ***rac*-4**/***meso*-4** in various solvents. A concentrated benzene-d_6 solution was prepared using a recrystallized sample of ***rac*-4**/***meso*-4** (1.0:0.1 isomeric ratio). Upon standing for 5 weeks at 22 °C, single crystals suitable for X-ray diffraction were obtained (Fig. 7).

One unusual feature of this structure is that the $\{PhN(CH_2)_3NPh\}$ chelate adopts a conformation intermediate between the idealized twist and envelope forms. Ref. [6e] reports the following trends in displacement of atoms from the N(1)–Zr–N(2) plane for idealized twist and envelope conformers of the $\{PhN(CH_2)_3NPh\}$ chelate: twist (−, +, 0, −, +) and envelope (−, +, 0, 0, 0), (where + is above; 0 is in; − is below the N(1)–Zr–N(2) plane). The displacement of atoms in our system (−, −, +, −, +) is intermediate between these two idealized conformers, with the following deviations in Å of C atoms from the N(1)–Zr–N(2) plane: C(34) –0.43, C(27) −0.41, C(26) +0.51, C(25) −0.94, C(28) +0.78. Similar to ***rac*-3**, the cyclopentadienyl rings of ***rac*-4** tend towards η^3-coordination, evidenced by the 2.4958–2.7317 Å range of Zr–C(cyclopentadienyl) bond lengths. The centroid–Zr–centroid angle (γ = 120.6°), interplanar ring angle (α = 70.5°), Cp(normal)–Cp(normal) dihedral angle (β = 109.5°), and tilt angle (τ = 5.6°) for ***rac*-4** have less tendency towards the characteristic angles of a doubly-linked zirconocene as compared to those for ***rac*-3**. However, the N(1)–Zr–N(2) angle of 89.45(6)° is small in comparison to that of ***rac*-3** (93.95(9)°), *meso*-$Me_2Si(3\text{-}t\text{-}Bu\text{-}C_5H_3)_2Zr\{PhN(CH_2)_3NPh\}$ (95.34(10)°) [6c] and *rac*-$Me_2Si(3\text{-}t\text{-}Bu\text{-}C_5H_3)_2Zr\{Me_3SiN(CH_2)_3NSiMe_3\}$ (92.63(8)°) [6c].

We followed the course of this metallation reaction at low temperature (0 °C) using ^{31}P NMR spectroscopy (with an unlocked NMR sample). Upon thawing a frozen sample of **2** and $Zr\{PhN(CH_2)_3NPh\}Cl_2(THF)_2$ in diethyl ether solvent, peaks are immediately observed corresponding to the *meso* and *rac* isomers as well as another species (vide supra). Though slightly broadened, these peaks appear in a similar relative ratio as observed in the preparative scale metallation depicted in Eq. (2). This experiment, along with the preferential crystallization of ***rac*-4** from solutions of ***rac*-4**/***meso*-4**, suggest that the $Zr\{PhN(CH_2)_3NPh\}Cl_2(THF)_2$/diethyl ether combination is not an appropriate choice for preparative scale isolation of pure ***meso*-4**.

Our observation that NMR samples of isolated ***rac*-3**/***meso*-3** in tetrahydrofuran-d_8 (initial ratio of 1.0:0.46) slowly change over the course of weeks at 22 °C to afford a sample that is solely ***rac*-3** led us to undertake careful NMR isomerization studies for both ***rac*-3**/***meso*-3** and ***rac*-4**/***meso*-4** at elevated temperature (60 °C) in tetrahydrofuran-d_8 solvent. All of these experiments were carried out in the dark to rule out the possibility of photochemically promoted isomerization. In each case, the *rac*/*meso* ratio was monitored using ^{31}P NMR spectroscopy, with frequent data sampling for the first 12 h, and daily monitoring until an equilibrium state was reached.

As described in Fig. 8, the ***rac*-3**/***meso*-3** ratio was monitored with no additive, with 2 equiv. KCl, and with 2 equiv. nBu$_4$NCl additive present. While the presence of KCl causes an initial drop in the percentage of ***meso*-3**, over time the rate of decay mimics that observed in the absence of KCl. It should be noted that solid KCl is apparent at the bottom of the NMR tube both before and after NMR monitoring; we assume that the KCl is at best sparingly soluble under reaction conditions. Both samples are completely converted to 100% ***rac*-3** over the course of 2 d at 60 °C. In contrast, addition of nBu$_4$NCl immediately converts the sample to 100% ***rac*-3**. Also, a color change is immediately observed in the presence of nBu$_4$NCl (yellow → orange solution). We invoke solubility and ion pairing effects to account for the differing kinetics of *rac* to *meso* isomerization in the presence of KCl and nBu$_4$NCl.

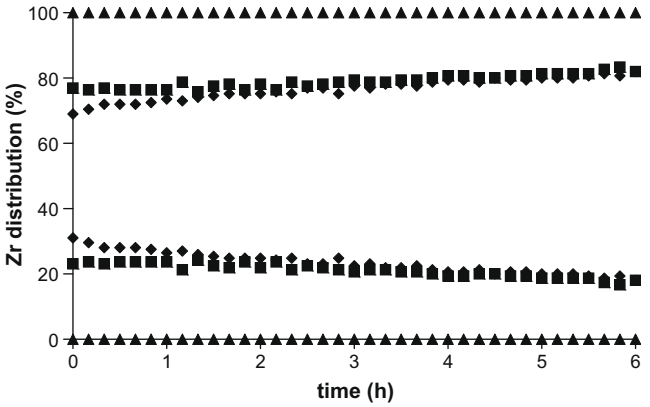

Fig. 8. Conversion of ***meso*-3** to ***rac*-3** starting from a 0.46:1.0 ***meso*-3**/***rac*-3** mixture (THF-d_8, 60 °C, in the dark); percentage of ***rac*-3** (upper curves) and ***meso*-3** (lower curves) plotted vs. time. Run i (diamonds), no additive; run ii (squares), 2 equiv. KCl (sparingly soluble); run iii (triangles), 2 equiv. nBu$_4$NCl.

Similar experiments using ***rac*-4**/***meso*-4** are depicted in Fig. 9. In this case, the *meso* isomer is the major isomer at the start of the experiments (1.0:0.24 ***meso*-4**/***rac*-4**). Here we observed similar behavior in the both the presence and absence of KCl, with negligible isomerization over the course of 12 h at 60 °C. In fact, a full week at 60 °C is required to obtain a 1.0:1.0 ratio of ***rac*-4**/***meso*-4**. In contrast, addition of nBu$_4$NCl immediately converts the sample to a 1.0:0.16 ratio of ***rac*-4**/***meso*-4**, and this ratio is maintained over the course of days at 60 °C. This appears to be the equilibrium ratio. A subtle color change is immediately observed in the presence of nBu$_4$NCl (orange-red → red solution).

The observed rate constant for isomerization, k_{obs}, was determined for Fig. 8, run i, and for Fig. 9, run i. Each experiment was treated as an approach to equilibrium system. A plot of $[-\ln\{(X_{t=t} - X_{t=\infty})/(X_{t=0} - X_{t=\infty})\}]$ versus time (in s), where X is the mole fraction of *meso* isomer, affords k_{obs} from the slope. The k_{obs} value for ***meso*-4** to ***rac*-4** isomerization ($k_{obs} = 1.2 \times 10^{-6}$ s^{-1}) is more than 15 fold smaller than that for ***meso*-3** to ***rac*-3** isomerization ($k_{obs} = 2.0 \times 10^{-5}$ s^{-1}). Both of these k_{obs} values are small in comparison to those reported by Hollis [22], Fu [23], and Curnow [24] for other metallocenes that incorporate phosphorus in their ligand arrays, albeit not as a component of an interannular linker. Indeed, the k_{obs} value for ***meso*-3** to ***rac*-3** isomerization in THF-d_8 at 60 °C has the same order of magnitude as Curnow's k_{obs} value ($1.59(3) \times 10^{-5}$ s^{-1}) for

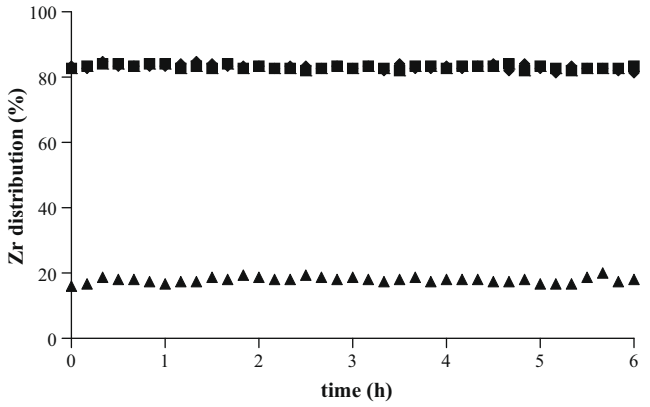

Fig. 9. Conversion of ***meso*-4** to ***rac*-4** starting from a 1.0:0.24 ***meso*-4**/***rac*-4** mixture (THF-d_8, 60 °C, in the dark); percentage of ***meso*-3** plotted vs. time. Run i (diamonds), no additive; run ii (squares), 2 equiv. KCl (sparingly soluble); run iii (triangles), 2 equiv. nBu$_4$NCl.

meso to *rac* isomerization of bis(1-diphenylphosphino-η^5-indenyl)iron(II) in THF-d_8 at 23 °C [24b].

A priori, we expected chloride catalyzed *rac* to *meso* isomerization to occur for our ***rac*-3**/***meso*-3** and ***rac*-4**/***meso*-4** mixtures, as described by Jordan for related dimethylsilyl linked zirconocenes [6f]. Therefore, in the presence of chloride additive, we postulate that one operating mechanism for equilibration of our *rac/meso* mixtures involves displacement of one cyclopentadienyl ligand by chloride, P–C bond rotation, chloride loss, and cyclopentadienyl ligand recoordination, analogous to Jordan's proposed mechanism (Scheme 2, where Nu$^-$ is chloride). However, the fact that we observe *rac* to *meso* isomerization in the absence of an additive raises the possibility of a second potential mechanism. We propose another nucleophile catalyzed mechanism, with the phosphine interannular linker acting as a nucleophile instead of chloride. Specifically, this second mechanism involves intramolecular displacement of one cyclopentadienyl ligand by the phosphine interannular linker (along with coordination of tetrahydrofuran solvent), P–C bond rotation, phosphine and tetrahydrofuran loss, followed by cyclopentadienyl ligand recoordination (Scheme 2). We suggest that the second cyclopentadienyl ligand may undergo a ring slip ($\eta^5 \rightarrow \eta^3$) to put the phosphine interannular linker in a more appropriate location (relative to zirconium) for intramolecular coordination. However, we realize it is difficult to rule out isomerization catalyzed by a negligible amount of adventitious chloride or water (a potential source of hydroxide) in our solutions of ***rac*-3**/***meso*-3** and ***rac*-4**/***meso*-4**. Regardless of the operating mechanism(s) of isomerization, the ability to isolate pure ***rac*-3** and pure ***rac*-4** via controlled isomerization of *rac*/*meso* mixtures (with no additive required) is valuable for our proposed future work in the realm of α-olefin polymerization (vide supra).

3. Summary

The syntheses of *rac/meso*-{PhP(3-*t*-Bu-C_5H_3)$_2$}Zr{SiMe$_3$N-(CH$_2$)$_3$NSiMe$_3$} (***rac*-3**/***meso*-3**, 2:1 ratio) and *rac/meso*-{PhP(3-*t*-Bu-C_5H_3)$_2$}Zr{PhN(CH$_2$)$_3$NPh} (***rac*-4**/***meso*-4**, 0.36:1.0 ratio) underscore the influence of the interannular linker in the course of metallation when Jordan's Zr{RN(CH$_2$)$_3$NR}Cl$_2$(THF)$_2$ (where R = SiMe$_3$ or Ph, respectively) is used as a metallation agent. Both ***rac*-3** and ***rac*-4** display tendencies towards η^3-coordination of their cyclopentadienyl rings, as evidenced by X-ray crystallography. Since mixtures of ***rac*-3**/***meso*-3** and ***rac*-4**/***meso*-4** equilibrate both in the presence and absence of chloride additive, we suggest a general isomerization mechanism involving nucleophile catalyzed displacement of one cyclopentadienyl ligand (where Nu$^-$ is chloride or the phosphine interannular linker). The ability to carry out controlled isomerization of *rac/meso* mixtures of **3** and **4** in the absence of additive is synthetically useful, irrespective of mechanism. Conversions of pure ***rac*-3** and ***rac*-4** to the corresponding zirconocene dichloride precatalyst and subsequent α-olefin polymerization studies are underway and will be reported in due course.

4. Experimental

4.1. General considerations

All chemical reactions were carried out under an atmosphere of argon using standard Schlenk techniques [28] unless otherwise noted. Argon gas was purified by passage over Drierite™. All chemicals were purchased from Aldrich and used as received unless otherwise noted. Dichlorophenylphosphine was purchased from Strem. ZrCl$_2$(THF)$_2${PhN(CH$_2$)$_3$NPh} [6b,6c,29], ZrCl$_2$(THF)$_2${Me$_3$

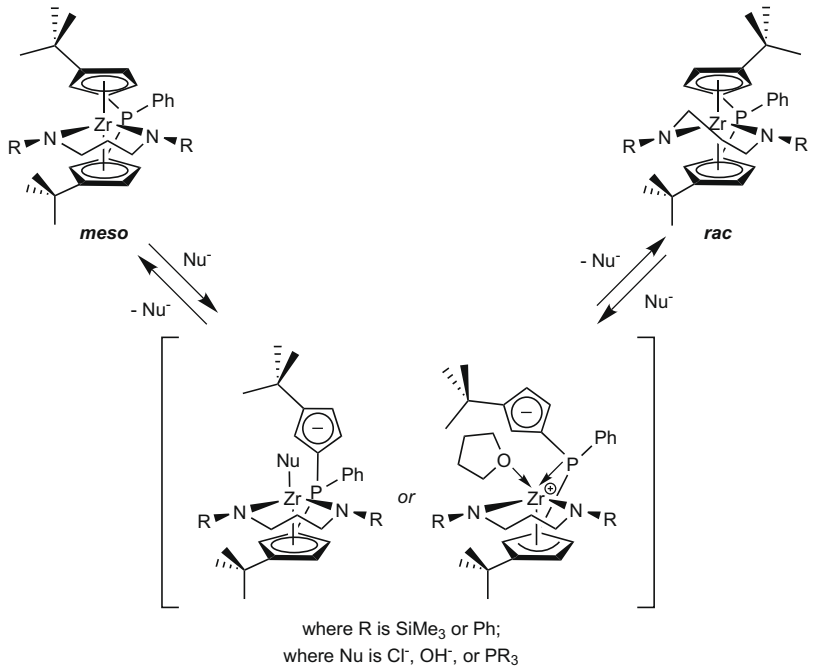

Scheme 2.

$SiN(CH_2)_3NSiMe_3$} [30], and Li(*t*-Bu-C_5H_4) [27] were prepared according to literature methods. Benzene-d_6 and tetrahydrofuran-d_8 were purchased from Cambridge Isotope Laboratories and dried over molecular sieves (8–12 mesh, 4 Å, activated) before use. An MBraun Manual Solvent Purification System (MB-SPS) was used to obtain the following anhydrous solvents: toluene, tetrahydrofuran, diethyl ether, pentane, and dichloromethane; solvents were submitted to three freeze-pump-thaw cycles before use [31]. Benzene was dried over sodium/benzophenone ketyl and stored under vacuum. Molecular sieves (8–12 Mesh, 4 Å) were purchased from J.T. Baker and activated before use. Potassium *tert*-butoxide was purchased from Aldrich and sublimed before use.

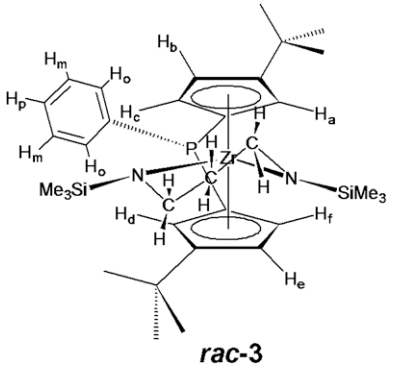

NMR spectra were recorded on a Varian Mercury spectrometer at 300 MHz (^{1}H), 75 MHz (^{13}C), and 121 MHz (^{31}P) at 298 K. ^{1}H and ^{13}C chemical shifts are referenced relative to the NMR solvent (residual protio solvent peak(s)); ^{31}P chemical shifts are referenced relative to phosphoric acid and triphenylphosphine oxide. The following abbreviations are used for NMR splitting patterns: pt (pseudo triplet) and br s (broad singlet). Elemental analyses were performed at Atlantic Microlab, Inc. in Norcross, Georgia.

4.2. Preparation of PhP(3-t-Bu-C_5H_4)$_2$ (**1**)

A 100-mL Schlenk flask was charged with Li(*t*-Bu-C_5H_4) (3.01 g, 23.5 mmol, 2.0 equiv.), tetrahydrofuran (20 mL), and pentane (7 mL). A 50-mL Schlenk flask was charged with $PhPCl_2$ (1.60 mL, 11.8 mmol, 1.0 equiv.) and tetrahydrofuran (7 mL). The Li(*t*-Bu-C_5H_4) solution was cooled to −78 °C, followed by dropwise addition of the $PhPCl_2$ solution via cannula transfer. The −78 °C dry ice/acetone bath was left intact to allow the reaction mixture to slowly warm to 22 °C over the course of 18 h. Solvent was removed in vacuo and pentane (30 mL) was added inside the glove box to provide an orange-brown slurry. Vacuum filtration and pentane washes (5 × 8 mL) provided a brown filtrate, which was concentrated in vacuo to yield **1** as a light brown oil (3.73 g, 90.2% yield). ^{1}H NMR (benzene-d_6, 22 °C): δ 7.45–7.68 (m, C_6H_5), 6.98–7.14 (m, C_6H_5), 6.70 (m, C_5H_4), 6.31–6.39 (m, C_5H_4), 6.05 (m, C_5H_4), 5.99 (m, C_5H_4), 4.02 (m, allylic C_5H_4), 3.11 (m, allylic C_5H_4), 3.07 (br s, allylic C_5H_4), 3.06 (m, allylic C_5H_4), 3.01 (m, allylic C_5H_4), 2.98 (m, allylic C_5H_4), 2.78 (m, allylic C_5H_4), 1.09 (s, C(CH_3)), 1.08 (s, C(CH_3)), 1.07 (s, C(CH_3)), 1.06 (s, C(CH_3)), 1.04 (s, C(CH_3)), 0.99 (s, C(CH_3)), 0.98 (s, C(CH_3)), 0.97 (s, C(CH_3)), 0.96 (s, C(CH_3)). ^{13}C{^{1}H} NMR (benzene-d_6, 22 °C): δ 141.5–143.1, 132.8–133.6, 124.8–125.2, 44.1–44.3, 43.4–43.8, 41.8–42.0, 33.7, 32.4, 31.2, 31.1, 30.1. ^{31}P{^{1}H} NMR (benzene-d_6, 22 °C): δ −18.7, −18.8, −19.1, −29.1, −29.2, −30.5, −30.6 (relative integrations for these peaks: 0.18. 0.08, 0.08, 0.48, 1.00, 0.24, and 0.27, respectively).

4.3. Preparation of K_2{PhP(3-t-Bu-C_5H_3)$_2$} (**2**)

A 100-mL Schlenk flask was charged with PhP(3-*t*-Bu-C_5H_4)$_2$ (3.73 g, 10.6 mmol, 1.0 equiv.) and tetrahydrofuran (25 mL), then cooled to 0 °C with stirring. In a separate Schlenk flask, potassium *tert*-butoxide (2.58 g, 23.0 mmol, 2.16 equiv.) was dissolved in tetrahydrofuran (15 mL), followed by dropwise transfer of this solution to the PhP(3-*t*-Bu-C_5H_4)$_2$ solution, with stirring at 0 °C. The 0 °C ice-water bath was left intact to slowly warm to 22 °C; After 30 min of stirring at 0 °C, precipitate began to form, yielding a pale peach-colored slurry. After 72 h of stirring, the reaction mixture

was concentrated to dryness, followed by continued drying in vacuo with heating to 50 °C for 3.5 h to remove residual solvent and *tert*-butanol byproduct. Inside the glove box, tetrahydrofuran (75 mL) was added to provide a pale peach-colored slurry. This slurry was transferred to a jar and cooled to −35 °C for 1 week. At this point, a white solid and red colored supernatant were present. Vacuum filtration yielded a white solid, which was transferred to a pear-shaped flask for drying in vacuo for 1 h. Compound **2** was isolated as a white powder (4.27 g, 70.1% yield). ^{1}H NMR analysis revealed the presence of nonstoichiometric protio THF (1.3 equiv.); this residual solvent was taken into account for percent yield calculations. Satisfactory elemental analysis data has not been obtained to date; poor solubility in THF has precluded preparative scale recrystallizations for elemental analysis purposes. ^{1}H NMR (THF-d_8, 22 °C): δ 7.80 (pt, J = 6.8 Hz, 2H, *ortho*-C_6H_5), 7.07 (pt, J = 7.4 Hz, 2H, *meta*-C_6H_5), 6.91 (pt, J = 6.9 Hz, 1H, *para*-C_6H_5), 5.81 (br s, 4H, two overlapping signals, C_5H_3), 5.57 (br s, 2H, C_5H_3), 3.62 (t, C_4H_8O), 1.78 (t, C_4H_8O), 1.15 (s, 18H, C(CH_3)$_3$). ^{13}C{^{1}H} NMR (THF-d_8, 22 °C): δ 132.2 (J = 14.9 Hz, *ortho*-C_6H_5), 126.8 (*meta*-C_6H_5), 123.8 (*para*-C_6H_5), 111.9 (J = 21.2 Hz, C_5H_3), 108.3 (J = 23.5 Hz, C_5H_3), 103.2 (J = 8.5 Hz, C_5H_3), 67.3 (C_4H_8O), 33.9 (C(CH_3)$_3$), four ipso carbon resonances not detected due to poor solubility of **2**. ^{31}P{^{1}H} NMR (THF-d_8, 22 °C): δ −31.1.

4.4. Preparation of rac/meso-{PhP(3-t-Bu-C_5H_3)$_2$}Zr{$Me_3SiN(CH_2)_3NSiMe_3$} (**rac-3/meso-3**)

A 250-mL Schlenk flask was charged with K_2{PhP(3-*t*-Bu-C_5H_3)$_2$}·1.3 THF (1.00 g, 1.93 mmol, 1.0 equiv.) and $ZrCl_2(THF)_2${$Me_3SiN(CH_2)_3NSiMe_3$} (0.87 g, 1.93 mmol, 1.0 equiv.), degassed, and cooled to −78 °C. Tetrahydrofuran (50 mL) was added by vacuum transfer, yielding a pale yellow slurry. The −78 °C dry ice/acetone bath was replaced by a 0 °C ice-water bath, and the reaction mixture was allowed to slowly warm to 22 °C. Upon warming, the reaction mixture took on a lemon-yellow color and opaque appearance. After 27.5 h, the reaction mixture was concentrated to dryness, and then dried in vacuo for an additional 1.5 h. Inside the glove box, pentane (40 mL) was added and the product mixture left to stir for 1 h. The product mixture was subjected to vacuum filtration to yield a yellow filtrate. The filtrate was then passed through a pad of celite, and finally though a disposable pipet containing a Kimwipe plug. The resulting yellow filtrate was concentrated to dryness and dried in vacuo for an additional 2.5 h to provide ***rac*-3**/***meso*-3** as a yellow, microcrystalline solid (0.89 g, 70.2% yield). Single crystals of ***rac*-3** for X-ray diffraction study were obtained from a pentane solution of ***rac*-3**/***meso*-3** cooled to −35 °C for 8 days. ^{31}P{^{1}H} NMR (benzene-d_6, 22 °C): δ −43.6 (*meso*), −37.1 (*rac*). 0.46:1.00, initial *meso:rac* ratio. ^{31}P{^{1}H} NMR (THF-d_8, 22 °C): δ −40.3 (*meso*), −33.8 (*rac*). Anal. Calc. for $C_{33}H_{53}N_2PSi_2Zr$: C, 60.41; H, 8.14; N, 4.27. Found: C, 59.46; H, 8.27; N, 4.21%.

rac isomer: ^{1}H NMR (benzene-d_6, 22 °C): δ 7.76 (pt, J = 7 Hz, 2H, H_o), 7.18 (m, 2H, H_m), 6.98 (t, J = 6 Hz, 1H, H_p), 6.84 (t, J = 3 Hz, 1H, H_b), 6.52 (dt, J = 3 Hz, 3 Hz, 1H, H_e), 6.42 (dt, J = 3 Hz, 3 Hz, 1H, H_f), 6.31 (dt, J = 3 Hz, 3 Hz, 1H, H_a), 5.87 (dt, J = 3 Hz, 3 Hz, 1H, H_d), 5.84 (dt, J = 3 Hz, 3 Hz, 1H, H_c), 3.35 (dd, J = 15.7 Hz, 4.5 Hz, 1H, NCH_2), 3.23 (dd, J = 15.1 Hz, 4.9 Hz, 1H, NCH_2), 3.03 (ddd, J = 15.7 Hz, 10.6 Hz, 4.8 Hz, 1H, NCH_2), 2.94 (ddd, J = 15.1 Hz, 10.9 Hz, 5.4 Hz, 1H, NCH_2), 1.21 (s, 9H, top ring C(CH_3)$_3$), 1.05 (s, 9H, bottom ring C(CH_3)$_3$), 1.03 (m, 1H, NCH$_2$CH_2), 0.94 (m, 1H, NCH$_2$CH_2), 0.26 (s, 9H, top ring Si(CH_3)$_3$), 0.07 (s, 9H, bottom ring Si(CH_3)$_3$). *Note*: NCH_2 resonances at 3.35 ppm and 3.03 ppm are on the same carbon; NCH_2 resonances at 3.23 ppm and 2.94 ppm are on the same carbon. ^{1}H NMR (THF-d_8, 22 °C): δ 7.68 (pt, J = 6.8 Hz, 2H, H_o), 7.40 (pt, J = 6.8 Hz, 2H, H_m), 7.32 (m, 1H, H_p), 6.83 (t, J = 2.6 Hz, 1H, C_5H_3), 6.49 (m, 1H, C_5H_3), 6.23 (m, 2H, *two overlapping resonances,* C_5H_3), 5.79 (dt, J = 2.6 Hz, 4.2 Hz, 1H, C_5H_3), 5.66 (dt, J = 2.6 Hz, 4.2 Hz, 1H, C_5H_3), 3.14–3.42 (m, 2H, NCH_2), 2.86–3.10 (m, 2H, NCH_2), 1.27 (s, 9H, C(CH_3)$_3$), 1.13 (s, 9H, C(CH_3)$_3$), *NCH$_2$CH$_2$ resonances not detected*, 0.20 (s, 9H, Si(CH_3)$_3$), 0.02 (s, 9H, Si(CH_3)$_3$). ^{13}C{^{1}H} NMR (benzene-d_6, 22 °C): δ 131.2 (J = 14 Hz, C_o), 128.8 (J = 4 Hz, C_m), 128.0 (C_p), 118.1 (J = 39 Hz, C_a), 118.1 (C_b), 110.7 (J = 39 Hz, C_f), 110.4 (J = 10 Hz, C_e), 106.6 (J = 7 Hz, C_c), 104.7 (J = 7 Hz, C_d), *C*(CH_3)$_3$ *resonances not detected*, 46.3 (NCH_2), 45.7 (NCH_2), 31.4 (C(CH_3)$_3$), 31.0 (C(CH_3)$_3$), 28.6 (NCH$_2$$CH_2$), 4.1 (Si($CH_3$)$_3$), 3.1 (Si($CH_3$)$_3$). ^{13}C{^{1}H} NMR (THF-d_8, 22 °C): δ 131.5 (J = 14 Hz, C_o), 129.1 (J = 4 Hz, C_m), 128.3 (C_p), 118.8 (C_b), 118.6 (J = 41 Hz, C_a), 111.0 (J = 40 Hz, C_f), 110.8 (J = 10 Hz, C_e), 107.1 (J = 7 Hz, C_c), 105.1 (J = 7 Hz, C_d), 46.7 (NCH_2), 46.1 (NCH_2), (*C*(CH_3)$_3$) *resonances not detected*, 31.6 (C(CH_3)$_3$), 31.2 (C(CH_3)$_3$), 29.1 (NCH$_2$$CH_2$), 4.0 (Si($CH_3$)$_3$), 3.1 (Si($CH_3$)$_3$).

meso isomer: ^{1}H NMR (benzene-d_6, 22 °C): δ 7.76 (m, 2H, H_o), 7.08 (m, 2H, H_m), 6.98 (m, 1H, H_p), 6.60 (m, 2H, Cp-*H*), 6.46 (m, 2H, Cp-*H*), 6.09 (m, 2H, Cp-*H*), 2.82–3.06 (m, 4H, NCH_2), 1.24 (s, 18H, C(CH_3)$_3$), *NCH$_2$CH$_2$ resonances not detected*, 0.27 (s, 9H, Si(CH_3)$_3$), −0.04 (s, 9H, Si(CH_3)$_3$). ^{1}H NMR (THF-d_8, 22 °C): δ 7.56 (pt, J = 6.8 Hz, 2H, H_o), 7.32 (m, 2H, H_m), 7.26 (m, 1H, H_p), 6.56 (dd, J = 2.4 Hz, J = 3.2 Hz, 2H, C_5H_3), 6.49 (m, 2H, C_5H_3), 6.08 (m, 2H, C_5H_3), 3.14–3.42 (m, 2H, NCH_2), 2.86–3.10 (m, 2H, NCH_2), 1.29 (s, 18H, C(CH_3)$_3$), *NCH$_2$CH$_2$ resonances not detected*, 0.21 (s, 9H, Si(CH_3)$_3$), 0.11 (s, 9H, Si(CH_3)$_3$). ^{13}C{^{1}H} NMR (benzene-d_6, 22 °C), selected resonances: δ 39.9, 39.8, 22.9, 0.41 (presumably two coincident peaks, Si(CH_3)$_3$). ^{13}C{^{1}H} NMR (THF-d_8, 22 °C), selected resonances: 46.7, 46.5, 45.4, 3.5 (Si(CH_3)$_3$), 1.6 (Si(CH_3)$_3$).

4.5. Preparation of rac/meso-{PhP(3-t-Bu-C_5H_3)$_2$}Zr{$PhN(CH_2)_3NPh$} (**rac-4/meso-4**)

A 250-mL round bottom flask was charged with K_2{PhP(3-*t*-Bu-C_5H_3)$_2$}·1.3 THF (0.32 g, 0.63 mmol, 1.01 equiv.) and $ZrCl_2(THF)_2${$PhN(CH_2)_3NPh$} (0.33 g, 0.62 mmol, 1.00 equiv.), topped with a 180° needle valve, removed from the glove box, degassed on the Schlenk line, and cooled to −78 °C. Diethyl ether (30 mL) was added by vacuum transfer, yielding a yellow slurry. The −78 °C dry ice/acetone bath was replaced by a 0 °C ice-water bath, and within 5 min the slurry became bright orange in color. The temperature was maintained at 0 °C for 2 h, followed by removal of solvent in vacuo and drying of the resulting orange residue for an additional 45 min. Inside the glove box, pentane (30 mL) was added and the product mixture was subjected to vacuum filtration (using a fine porosity fritted funnel) to yield an orange filtrate. Pentane washes (4 × 2 mL) were used and the washes also passed through the fritted funnel. The filtrate was concentrated to dryness and dried in vacuo for an additional 1 h to provide ***rac*-4**/***meso*-4** as an orange, microcrystalline solid (0.29 g, 66.4% yield). ^{31}P{^{1}H} NMR (benzene-d_6, 22 °C): δ −38.7 (*meso*), −35.8 (*rac*), −24.6 (minor species). 1.00:0.36:0.24, *meso:rac:*minor species ratio. ^{31}P{^{1}H} NMR (THF-d_8, 60 °C): δ −38.7 (*meso*), −35.6 (*rac*), −24.5 (minor species). Single crystals of ***rac*-4** for X-ray diffraction study were obtained from a concentrated benzene-d_6 solution of ***rac*-4**/***meso*-4** (recrystallized material, 1.0:0.1 isomeric ratio) that was stored for 5 weeks at 22 °C. Anal. Calc. for $C_{39}H_{45}N_2PZr$: C, 70.55; H, 6.83; N, 4.22. Found: C, 71.17; H, 7.14; N, 3.77%. Notations for NMR peak assignments are as follows: phosphino-phenyl is ring A, one amino-phenyl is ring B, the other amino-phenyl is ring C, one cyclopentadienyl is ring D, and the other cyclopentadienyl is ring E.

rac isomer: ^{1}H NMR (benzene-d_6, 22 °C): δ 7.74 (pt, J = 7.2 Hz, 2H, H_o-*ring A*), 7.23 (t, J = 7.6 Hz, 2H, H_m-*ring B*), 7.13 (m, 2 H, H_m-*ring A*), 7.05 (m, 2H, H_m-*ring C*), 7.03 (m, 1H, H_p-*ring A*), 6.89 (t, J = 7.5 Hz, 1H, H_p-*ring B*), 6.86 (d, J = 7.9 Hz, 2H, H_o-*ring B*), 6.77 (t, J = 7.5 Hz, 1H, H_p-*ring C*), 6.55 (m, 1H, Cp-*H*-*ring D*), 6.50 (m, 1H,

Cp-*H-ring E*), 6.44 (d, *J* = 8.2 Hz, 2H, H_o-*ring C*), 6.30 (m, 1H, Cp-*H-ring D*), 6.12 (m, 1H, Cp-*H-ring D*), 5.91 (m, 1H, Cp-*H-ring E*), 5.87 (m, 1H, Cp-*H-ring E*), 3.26–3.60 (overlapping m, 4H, NCH_2), 1.43–1.72 (overlapping m, 2H, NCH_2CH_2), 0.97 (s, 9H, $C(CH_3)_3$), 0.94 (s, 9H, $C(CH_3)_3$). $^{13}C\{^1H\}$ NMR (benzene-d_6, 22 °C): δ 162.0 (ipso-amino-phenyl), 160.4 (ipso-amino-phenyl), 143.2 (ipso-*t*-Bu-Cp, *J* = 9.7 Hz), 138.4 (ipso-*t*-Bu-Cp, *J* = 6.7 Hz), *ipso-phosphino-phenyl resonance not detected*, 131.2 (*J* = 14.2 Hz, C_o-*ring A*), 128.9 (*J* = 4.4 Hz, C_m-*ring A*), 128.7 (C_m-*ring B*), 128.2 (C_p-*ring A*), 128.1 (C_m-*ring C*), 123.6 (ring D), 121.8 (C_o-*ring B*), 120.2 (C_p-*ring B*), 119.8 (C_o-*ring C*), 119.4 (C_p-*ring C*), 116.3 (*J* = 38.8 Hz, *ring D*), 114.9 (*J* = 38.8 Hz, *ring E*), 112.8 (*J* = 9.7 Hz, *ring E*), 108.4 (*J* = 8.5 Hz, *ring D*), 105.8 (*J* = 8.5 Hz, *ring E*), 105.1 (*J* = 19.1 Hz, *ring D*), 101.0 (*J* = 19.1 Hz, *ring E*), 55.6 (NCH_2), 55.0 (NCH_2), $C(CH_3)_3$ *resonances not detected*, 31.5 ($C(CH_3)_3$), 31.2 ($C(CH_3)_3$), 26.3 (NCH_2CH_2).

meso isomer: ^1H NMR (benzene-d_6): δ 7.72 (pt, *J* = 7 Hz, 2H, H_o-*ring A*), 7.20 (pt, *J* = 7 Hz, 2H, H_m-*ring A*), 7.0 (m, 1H, H_p-*ring A*), 6.4–7.8 (m, 10H, *Ph*$N(CH_2)_2N$*Ph*), 6.63 (m, 2H, Cp-*H*), 6.59 (d, *J* = 9.7 Hz, 2H, H_o-*amino-phenyl*), 6.59 (d, *J* = 9.7 Hz, 2H, H_o-*amino-phenyl*), 6.09 (m, 4H, Cp-*H*), 3.46 (t, *J* = 6 Hz, 2H, NCH_2), 3.29 (t, *J* = 6 Hz, 2H, NCH_2), 1.58 (t, *J* = 5 Hz, 2H, NCH_2CH_2), 0.88 (s, 18H, $C(CH_3)_3$). $^{13}C\{^1H\}$ NMR (benzene-d_6): δ 161.2, 144.9, 127–131 (overlapping resonances), 119.8, 113.0, 108.1, 53.9, 52.4, 33.1, 31.2, 29.1.

4.6. NMR monitoring of metallation to form ***rac-3/meso-3***

Inside the glove box, a J. Young NMR tube was charged with **2** (30 mg, 57 μmol), $ZrCl_2(THF)_2\{Me_3SiN(CH_2)_3NSiMe_3\}$ (26 mg, 57 μmol), and ferrocene (11 mg, 59 μmol, ^1H NMR internal standard). The upper portion (inside) of the NMR tube was wiped clean with a dry Kimwipe to remove residual solids and to allow the Teflon cap to make an air-tight seal. Using a Schlenk line, tetrahydrofuran-d_8 solvent (1.0 mL) was added via vacuum transfer at −196 °C. While the sample was still frozen, the NMR tube was immediately inserted into a thermostated probe of a Varian Mercury NMR spectrometer at 300 MHz at either 295 K or 243 K (see Section 2). For $^{31}P\{^1H\}$ NMR data acquisition, 128 transients were recorded for each experiment. Due to overlapping signals in the ^1H NMR spectra, $^{31}P\{^1H\}$ NMR was used to monitor the relative ratio of ***rac-3*** and ***meso-3***. The initial spectrum was recorded (*t* = 0) immediately. Initially, spectra were acquired every 10 min; after frequent monitoring for 2–3 h, 30 min intervals were used for spectral acquisition for a total of 8 h. The NMR tube was removed from the NMR spectrometer, stored at 22 °C in the dark, and subsequent spectra were acquired at approximately 12 h intervals until only ***rac-3*** remained.

4.7. NMR monitoring of metallation to form ***rac-4/meso-4***

Inside the glove box, a J. Young NMR tube was charged with **2** (33 mg, 64 μmol) and $ZrCl_2(THF)_2\{PhN(CH_2)_3NPh\}$ (35 mg, 66 μmol). Using a Schlenk line, protio diethyl ether solvent (1.0 mL) was added via vacuum transfer at −196 °C. While the sample was still frozen, the NMR tube was immediately inserted into a thermostated probe of a Varian Mercury 300 MHz NMR spectrometer at 273 K (see Section 2). The initial spectrum was recorded immediately (*t* = 0). For $^{31}P\{^1H\}$ NMR data acquisition, 128 transients were recorded for each experiment. Due to overlapping signals in the ^1H NMR spectra, $^{31}P\{^1H\}$ NMR was used to monitor the relative ratio of ***rac-4*** to ***meso-4***.

4.8. NMR monitoring of isomerization in the absence or presence of salts

Inside the glove box, a small vial was charged with either ***meso-3/rac-3*** (20 mg, 30 μmol, 0.46 (*meso*):1.00 (*rac*) ratio) or ***meso-4/rac-4*** (17 mg, 26 μmol, 1.00 (*meso*):0.36 (*rac*):0.24 (minor species) ratio). To a J. Young NMR tube was added either KCl (60 μmol, 2 equiv.), nBu$_4$NCl (60 μmol, 2 equiv.), or no additive. Using a microsyringe, tetrahydrofuran-d_8 solvent (0.7 mL) was added to the small vial containing ***rac-3/meso-3*** or ***rac-4/meso-4*** and the solution was immediately transferred to the J. Young NMR tube. The J. Young NMR tube was removed from the glove box, shaken vigorously, and inserted into a thermostated probe of a Varian Mercury 300 MHz NMR spectrometer at 333 K (see Section 2); overall, approximately 5 min elapsed between the addition of NMR solvent and insertion of the sample into the NMR probe. For $^{31}P\{^1H\}$ NMR data acquisition, 128 transients were recorded for each experiment. The initial spectrum was recorded immediately (*t* = 0). Spectra were acquired every 10 min for 6 h, and then every 15 min for an additional 6 h. The NMR tube was removed from the instrument and placed in a 60 °C constant temperature bath in the dark for continued heating. Subsequent spectra were acquired daily until the *rac/meso* equilibrium state was reached.

4.8. Single crystal X-ray structure determination

4.8.1. General

Crystallographic data are presented in Table 1. Single crystals of ***rac-3*** and ***rac-4***, respectively, were mounted using Paratone® oil

Table 1
Crystal data and structure refinement for ***rac-3*** and ***rac-4***

	rac-3	***rac-4***
Empirical formula	$C_{33}H_{53}N_2PSi_2Zr$	$C_{45}H_{51}N_2PZr$
Formula weight	656.14	742.07
Crystal color	Colorless	Yellow
Habit	Block	Blade
Temperature (K)	100(2)	100(2)
Wavelength (Å)	1.54178	1.54178
Crystal system	Monoclinic	Triclinic
Space group	*C*2/*c*	$P\bar{1}$
Unit cell dimensions		
a (Å)	28.6415(17)	10.2741(5)
α (°)	90	66.159(2)
b (Å)	17.7876(10)	14.4603(6)
β (°)	126.134(2)	84.658(2)
c (Å)	16.9360(10)	14.4648(6)
γ (°)	90	72.539(2)
Volume (Å^3)	6968.5(7)	1874.06(14)
Z	8	2
Density (calculated) (mg/m^3)	1.251	1.315
Absorption coefficient (mm^{-1})	3.842	3.053
F(000)	2784	780
Crystal size (mm^3)	0.20 × 0.16 × 0.13	0.15 × 0.15 × 0.07
Θ range for data collection	3.13–68.06°	4.51–69.81°
Index ranges	$-34 \leqslant h \leqslant 34$, $-21 \leqslant k \leqslant 18$, $-19 \leqslant l \leqslant 20$	$-12 \leqslant h \leqslant 12$, $-16 \leqslant k \leqslant 17$, $-16 \leqslant l \leqslant 17$
Reflections collected	37012	13609
Independent reflections [$R_{(int)}$]	6214 [0.0279]	6635 [0.0199]
Completeness to Θ = 67.00°	99.1 %	96.3 %
Absorption correction	Semi-empirical from equivalents	Semi-empirical from equivalents
Maximum and minimum transmission	0.6310 and 0.5152	0.8147 and 0.6574
Refinement method	Full-matrix least-squares on F^2	Full-matrix least-squares on F^2
Data/restraints/parameters	6214/0/364	6635/0/448
Goodness-of-fit (GOF) on F^2	1.050	1.031
Final *R* indices [$I > 2\sigma(I)$]	R_1 = 0.0385, wR_2 = 0.1009	R_1 = 0.0270, wR_2 = 0.0699
R indices (all data)	R_1 = 0.0400, wR_2 = 0.1020	R_1 = 0.0284, wR_2 = 0.0709
Largest difference peak and hole (e/Å^3)	1.512 and −0.468	0.583 and −0.345

onto a glass fiber and cooled to the data collection temperature of 100 K. Data were collected on a Brüker-AXS Kappa APEX II CCD diffractometer with 1.54178 Å Cu Kα radiation. Unit cell parameters were obtained from 90 data frames, 0.5° Φ, from three different sections of the Ewald sphere. For ***rac*-3**, the systematic absences in the diffraction data were consistent with the centrosymmetric monoclinic space group, $C2/c$. For ***rac*-4**, no higher symmetry than triclinic was evident from the diffraction data; solution in the centrosymmetric space group option $P\bar{1}$ yielded chemically reasonable and computationally stable results of refinement. The data-set was treated with SADABS absorption corrections based on redundant multi-scan data (Sheldrick, G., Brüker-AXS, 2001) $T_{max}/T_{min} = 1.22$ (for ***rac*-3**) and $T_{max}/T_{min} = 1.24$ (for ***rac*-4**). A single molecule was located in a general position yielding $Z = 8$ and $Z' = 1$ for ***rac*-3**; $Z = 2$ and $Z' = 1$ for ***rac*-4**. All non-hydrogen atoms were refined with anisotropic displacement parameters. All hydrogen atoms were treated as idealized contribution. For ***rac*-3**, the largest difference peak and hole of 1.512 and −0.468 e/Å^3 resulted from heavy atom noise around the zirconium atom.

Supplementary material

CCDC 697639 and 697640 contains the supplementary crystallographic data for ***rac*-3** and ***rac*-4**. These data can be obtained free of charge from The Cambridge Crystallographic Data Centre via www.ccdc.cam.ac.uk/data_request/cif.

Acknowledgments

Acknowledgment is made to the Donors of the American Chemical Society Petroleum Research Fund and Villanova University for support of this research. We thank Dr. Walter Boyko of Villanova University for his assistance with NMR spectroscopy. We acknowledge a reviewer's suggestions regarding the structural assignments for the ***rac*-4**/***meso*-4** reaction mixture.

References

[1] H.H. Brintzinger, D. Fischer, R. Mülhaupt, B. Rieger, R.M. Waymouth, Angew. Chem., Int. Ed. Engl. 34 (1995) 1143–1170.
[2] G.W. Coates, Chem. Rev. 100 (2000) 1223–1252.
[3] J.A. Smith, J.V. Seyerl, G. Huttner, H.H. Brintzinger, J. Organomet. Chem. 173 (1979) 175–185.
[4] C.E. Zachmanoglou, A. Docrat, B.M. Bridgewater, G. Parkin, C.G. Brandow, J.E. Bercaw, C.N. Jardine, M. Lyall, J.C. Green, J.B. Keister, J. Am. Chem. Soc. 124 (2002) 9525–9546.
[5] P.J. Shapiro, Coord. Chem. Rev. 231 (2002) 67–81.
[6] (a) X. Zhang, Q. Zhu, I.A. Guzei, R.F. Jordan, J. Am. Chem. Soc. 122 (2000) 8093–8094;
(b) M.D. LoCoco, X. Zhang, R.F. Jordan, J. Am. Chem. Soc. 126 (2004) 15231–15244;
(c) M.D. LoCoco, R.F. Jordan, Organometallics 22 (2003) 5498–5503;
(d) M.D. LoCoco, R.F. Jordan, J. Am. Chem. Soc. 126 (2004) 13918–13919;
(e) A.R. Dunn, L.E. Sweet, D.C. Wiser, M.D. LoCoco, R.F. Jordan, Organometallics 23 (2004) 5671–5680;
(f) R.M. Buck, N. Vinayavekhin, R.F. Jordan, J. Am. Chem. Soc. 129 (2007) 3468–3469.
[7] E.D. Brady, T.P. Hanusa, M. Pink, V.G. Young Jr., Inorg. Chem. 39 (2000) 6028–6037.
[8] N. Leyser, K. Schmidt, H.H. Brintzinger, Organometallics 17 (1998) 2155–2161.
[9] C. Freund, B. Martin-Vaca, G. Bouhadir, D. Bourissou, in: M.A. Cato (Ed.), Trends in Organometallic Chemistry Research, Nova Science Publishers, Hauppauge, NY, 2005, pp. 1–53.
[10] D. Bourissou, C. Freund, B. Martin-Vaca, G. Bouhadir, C.R. Chimie 9 (2006) 1120–1142.
[11] H.G. Alt, M. Jung, J. Organomet. Chem. 568 (1998) 127–131.
[12] J.H. Shin, T. Hascall, G. Parkin, Organometallics 18 (1999) 6–9.
[13] D.N. Kazul'kin, A.N. Ryabov, V.V. Izmer, A.V. Churakov, I.P. Beletskaya, C.J. Burns, A.Z. Voskoboynikov, Organometallics 24 (2005) 3024–3035.
[14] C.J. Schaverien, R. Ernst, W. Terlouw, P. Schut, O. Sudmeijer, P.H.M. Budzelaar, J. Mol. Catal. A: Chem. 128 (1998) 245–256.
[15] H. Kopf, N. Klouras, Monatsh. Chem. 114 (1983) 243–247.
[16] M. Häp, T. Gilles, T. Kruck, K.-F. Tebbe, Z. Naturforsch. 54b (1999) 482–486.
[17] (a) G.K. Anderson, M. Lin, Inorg. Chim. Acta 142 (1988) 7–8;
(b) G.K. Anderson, M. Lin, Organometallics 7 (1988) 2285–2288.
[18] J.H. Shin, B.M. Bridgewater, G.E. Parkin, Organometallics 19 (2000) 5155–5159.
[19] N. Leyser, K. Schmidt, H.H. Brintzinger, Organometallics 17 (1998) 2155–2161.
[20] K.A.O. Starzewski, M.W. Kelly, A. Stumpf, D. Freitag, Angew. Chem., Int. Ed. 38 (1999) 2439–2443.
[21] (a) O.J. Curnow, G. Huttner, S.J. Smail, M.M. Turnbull, J. Organomet. Chem. 524 (1996) 267–270;
(b) J.R. Butchard, O.J. Curnow, S.J. Smail, J. Organomet. Chem. 541 (1997) 407–416.
[22] (a) T.K. Hollis, L.-S. Wang, F. Tham, J. Am. Chem. Soc. 122 (2000) 11737–11738;
(b) T.K. Hollis, Y.J. Ahn, F.S. Tham, Chem. Commun. (2002) 2996–2997;
(c) T.K. Hollis, Y.J. Ahn, F.S. Tham, Organometallics 22 (2003) 1432–1436;
(d) Y.J. Ahn, R.J. Rubio, T.K. Hollis, F.S. Tham, B. Donnadieu, Organometallics 25 (2006) 1079–1083.
[23] S. Bellemin-Laponnaz, M.M.-C. Lo, T.H. Peterson, J.M. Allen, G.C. Fu, Organometallics 20 (2001) 3453–3458.
[24] (a) O.J. Curnow, G.M. Fern, Organometallics 21 (2002) 2827–2829;
(b) O.J. Curnow, G.M. Fern, M.L. Hamilton, A. Zahl, R. van Eldik, Organometallics 23 (2004) 906–912;
(c) O.J. Curnow, G.M. Fern, M.L. Hamilton, E.M. Jenkins, J. Organomet. Chem. 689 (2004) 1897–1910.
[25] P. Jutzi, Chem. Rev. 86 (1986) 983–996.
[26] (a) B.L. Zhu, B.Q. Wang, S.S. Xu, X.Z. Zhou, Youji Huaxue 23 (2003) 1049–1057;
(b) B.L. Zhu, B.Q. Wang, Chem. Abstr. (2003) 830385;
(c) D.L. Zubris, in: L.S. Baugh, J.M. Canich (Eds.), Stereoselective Polymerization with Single-Site Catalysts, CRC Press, Boca Raton, FL, 2008, pp. 101–134.
[27] T.A. Herzog, Ph.D. Thesis, California Institute of Technology, Pasadena, CA, 2007.
[28] D.F. Shriver, M.A. Drezdon, The Manipulation of Air-Sensitive Compounds, 2nd ed., Wiley, New York, 1986.
[29] J.H. Billman, L.R. Caswell, J. Org. Chem. 16 (1951) 1041–1046.
[30] (a) G. Courtois, L. Miginiac, J. Organomet. Chem. 340 (1988) 127–141;
(b) S. Friedrich, L.H. Gade, I.J. Scowen, M. McPartlin, Organometallics 14 (1995) 5344–5349.
[31] A.B. Pangborn, M.A. Giardello, R.H. Grubbs, R.K. Rosen, F.J. Timmers, Organometallics 15 (1996) 1518–1520.